

# The Technique of Changing Connectivity with Large Deformation Mesh for Lagrangian Method and Its Application

**Y. Hong, W. Ruili, L. Zhong**

[yuhong9s@sina.com](mailto:yuhong9s@sina.com)

**Institute of Applied Physics and computational mathematics, Beijing, China**

**This paper is supported by the National Natural Science Foundation of China  
( 11372051 , 91630312 ) and the grant of CAEP (2015B0202045 ).**

# Contents



IAPCM

- **Backgrounds**
- **Polygonal meshes and motivation**  
( **Structured.VS. Unstructured grids** )
- **The changing connectivity of mesh**  
( **FVM.VS. Changing connectivity** )
- **LAD2D CODE**
- **Three numerical examples**
- **Conclusions**

# Backgrounds(1)



IAPCM

- The main features of our problems (see figure 1).
  - Multi-Material ;
  - High temperature ;
  - High pressure ;
  - Large-deformation ;
  - Compressible fluid dynamics.

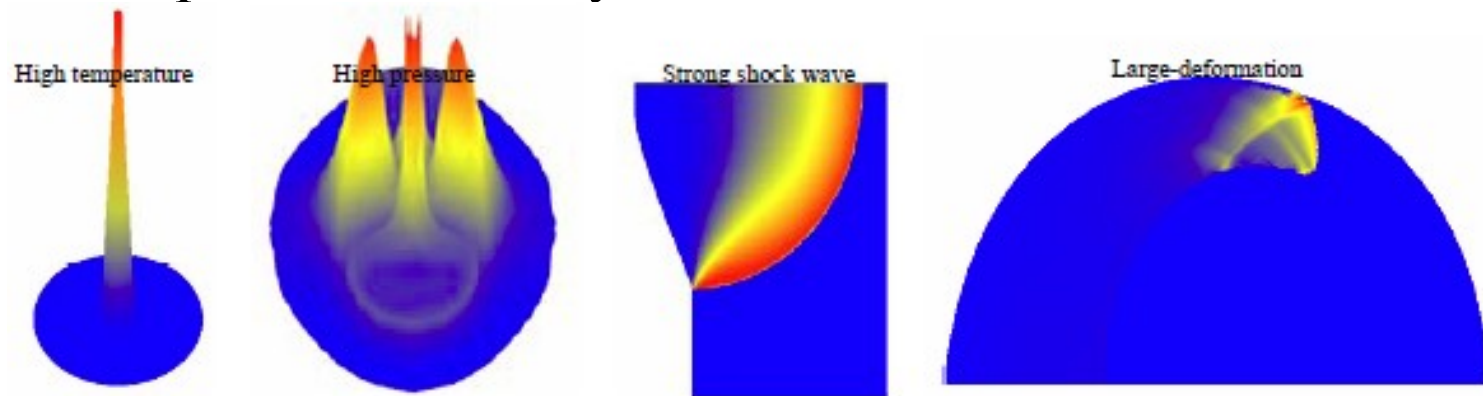


Fig.1 The characteristics of problems

➔ **Lagrangian method is essential for such problems !**

# Backgrounds(2)



➤ The 2D Cartesian Euler equations in non-conservative form

$$\frac{\partial \rho}{\partial t} + C \psi \rho \bar{u} = 0 \quad \text{Mass equation} \quad (1)$$

$$\frac{\partial \rho \bar{u}}{\partial t} + C \psi \rho \bar{u} \bar{u} + C P = 0 \quad \text{Momentum equation} \quad (2)$$

$$\frac{\partial \rho E}{\partial t} + C \psi \rho E \bar{u} + C \psi P \bar{u} = 0 \quad \text{Energy equation} \quad (3)$$

$$P = \begin{cases} P(\rho, e) & \text{Non explosive} \\ P(\rho, e, F) & \text{explosive} \end{cases} \quad \text{Equation of state} \quad (4)$$

$$\frac{d\lambda}{dt} = F(\rho, e, \lambda) \quad \text{Explosive reaction rate} \quad (5)$$

Where  $\rho$  denotes the density,  $\bar{u} = (u, v)^T$  is the velocity,  $e$  is the specific internal energy and  $P$  is the pressure,  $E = e + \frac{1}{2} \bar{u} \cdot \bar{u}$  is the total energy.

# Backgrounds(3)



## ➤ Burn function for explosive

the burn fractions  $F$  that control the release of chemical energy are computed by

$$F = [\max(F_1, F_2)]^{n_3} \quad (6)$$

Where  $F=0$  denotes no burning;  $0 < F < 1$  denotes burning;  $F=1$  denotes burning finished. Wilkins function  $F_1$  is:

$$F_1 = \begin{cases} 0, & V \geq V_0 \\ (V_0 - V)/(V_0 - V_J), & V_0 > V > V_J \\ 1, & V \leq V_J \end{cases} \quad (7)$$

C-J burn function  $F_2$  is:

$$F_2 = \begin{cases} 0, & t \leq t_3 \\ (t - t_3)/\Delta L, & t_3 < t < t_3 + \Delta L \\ 1, & t \geq t_3 + \Delta L \end{cases} \quad (8)$$



where  $V_J = \gamma W_0 / (\gamma + 1)$  denotes specific volume;  $V_0$  denotes initial volume;  $\gamma$  denotes the ratio of specific heats for air;  $t$  is current time;  $t_3$  is the burn-beginning time;  $\Delta L = v_3 \Delta R / D_J$ .  $\Delta R$  is cell width;  $D_J$  is the detonation velocity;  $\gamma$  is the ratio of specific heats;  $n_3$  and  $V_3$  are adjustable parameters.

# Backgrounds(4)



## ➤ Equation of state for explosive

The Jones-Wilkins-Lee (JWL) equation of state (EOS) is used for the reacted and un-reacted gases in the explosive regions. The EOS of the pressure-dependent JWL type is

$$P_{EOS} = A \left( 1 - \frac{\omega}{R_1 V} \right) e^{-R_1 V} + B \left( 1 - \frac{\omega}{R_2 V} \right) e^{-R_2 V} + \frac{\omega E}{V} \quad (9)$$

Where  $P_{EOS}$  is the pressure,  $V$  is relative specific volume,  $V = \frac{\rho_0}{\rho}$ ,  $E$  is the detonation energy per unit volume,  $E = \rho_0 e$ , and A, B, R1, R2 and  $\omega$  are constants to be calibrated. The calculated pressure of the shock wave by using JWL parameters determined by the numerical method agrees with experimental results.

# Backgrounds(5)



## ➤ Equation of state for metal material

Two equations of state (EOS) have been employed in the present work; the ‘stiffened gas’ EOS and Mie-Gruneisen EOS.

(1) The stiffened gas equation of state where the pressure  $P$  and sound speed  $c_s$  are given in terms of the density  $\rho$  and the specific internal energy  $e$  by

$$P = c_0^2(\rho - \rho_0) + (\gamma - 1)\rho e, \quad (10)$$

$$c_s = c_0 \left[ \gamma - (\gamma - 1) \frac{P_0}{\rho} \right] + \gamma(\gamma - 1)e. \quad (11)$$

(2) For a moderately realistic model, Mie-Gruneisen EOS has been used for the simulations of metal materials. It has following form:

$$P = \frac{\rho_0 C_0^2 \mu \left[ 1 + \left( 1 - \frac{\gamma_0}{2} \right) \mu \right]}{[1 - (S_\alpha - 1)\mu]^2} + \gamma_0 E, \quad \mu = \frac{\rho}{\rho_0} - 1 \quad (12)$$

where  $C_0$ 、 $S_\alpha$ 、 $\gamma_0$  are the Grunneisen constants.  $\rho_0$  denote the physical property parameters.

# Backgrounds(6)



IAPCM

- These are three main methods for high nonlinear partial differential equations in engineering design and basic science research: Lagrangian, Euler, ALE (Arbitrary Lagrange-Euler).
- **Eulerian methods** with fixed mesh are usually suitable for flow with large deformation, but are usually not suitable for multi-material fluids where interfaces among materials should be accurately.

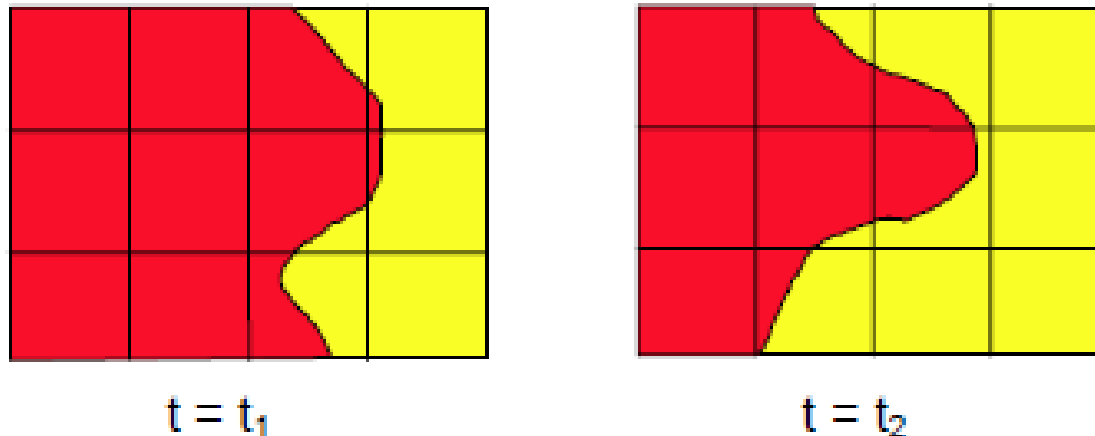


Fig.2 Euler Solver

# Backgrounds(7)



IAPCM

- **Lagrangian method** with mesh moves with the local fluid velocity is usually suitable for multi-material fluids to accurately capture interfaces among different.
- **Lagrangian method** is the most popular method and the main simulation tool in compressible fluid dynamics with multi-material flows of high temperature and high pressure.

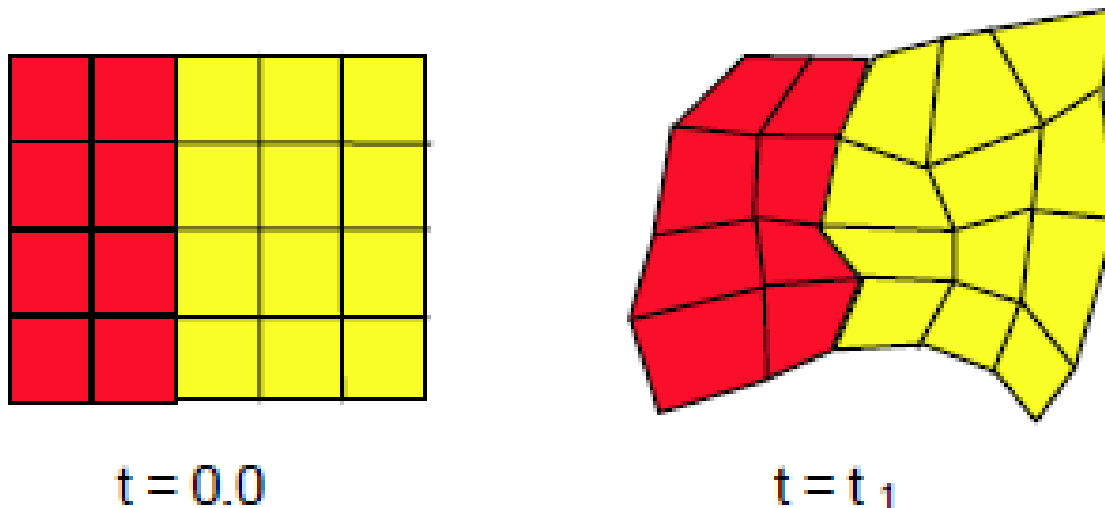


Fig.3 Lagrange Solver

# Backgrounds(8)



IAPCM

## ➤ Lagrangian method

- **Lagrangian methods** have the advantages of well-resolved material interfaces , but it is inevitable that the applications with a large shearing distortion lead to highly distorted cells. For example, mesh intersection, mesh tangling, large deformation (see Fig.4). These will reduce the accuracy of the discrete scheme , and the computation will run termination 。

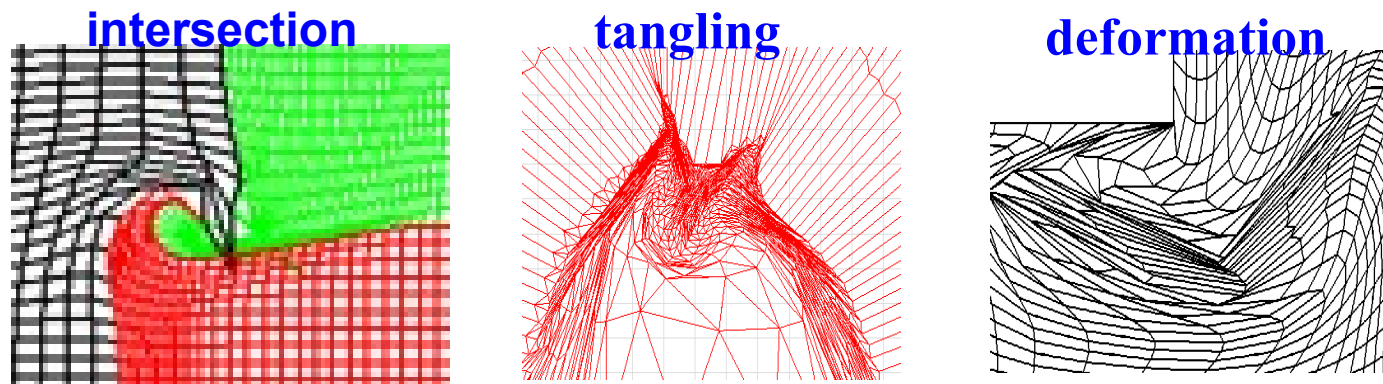


Fig.4 Examples of large deformation in computational grids

# Backgrounds(9)



IAPCM

## ➤ Purpose and motivation

- In this report, we propose an efficient computer code (LAD2D-Lagrangian Adaptive HydroDynamics Code in 2-D Space). LAD2D uses a Lagrangian finite volume numerical technique. The method manages the sliding meshes and the internal meshes unifying as arbitrary polygonal meshes. Spatial discretizations are formed with respect to a mesh of arbitrary polygonal unstructured cells. Of particular interest is **the changing connectivity of mesh technology** to handle the large deformation mesh and to close gap during numerical simulation processes.

# Polygonal meshes and motivation(1)

## ➤ Structured & Unstructured

- There are two main classes of grids. If the internal points are connected to their neighbours in a way independent of their position , the mesh is called structured. (Fig. 5a)
- When the pattern of the connections varies from point to point , the mesh is called unstructured. (Fig. 5b)

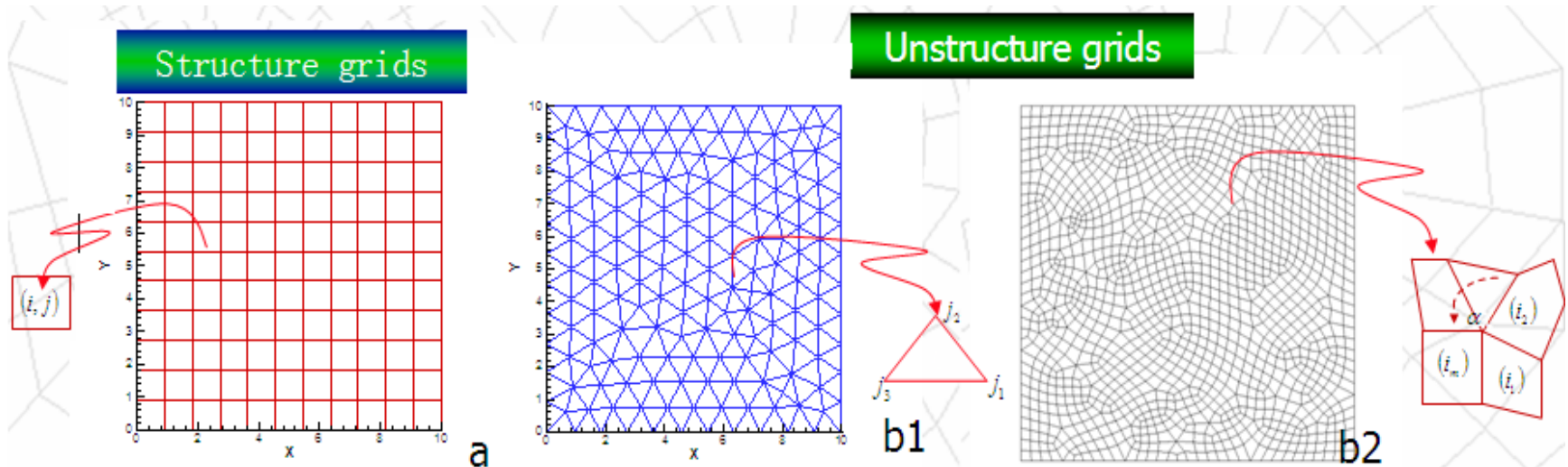


Fig.5 Definition of the grids

# Polygonal meshes and motivation(2)

## ➤ Structured & Unstructured

- In the structured grids, the connectivity of the grid is implicit. On the contrary, the connectivity of unstructured grids must be explicitly described by an appropriate data structure. unstructured grids can be crucial when dealing with domains of complex geometry or when the mesh has to be adapted to complicated features of the flow field.

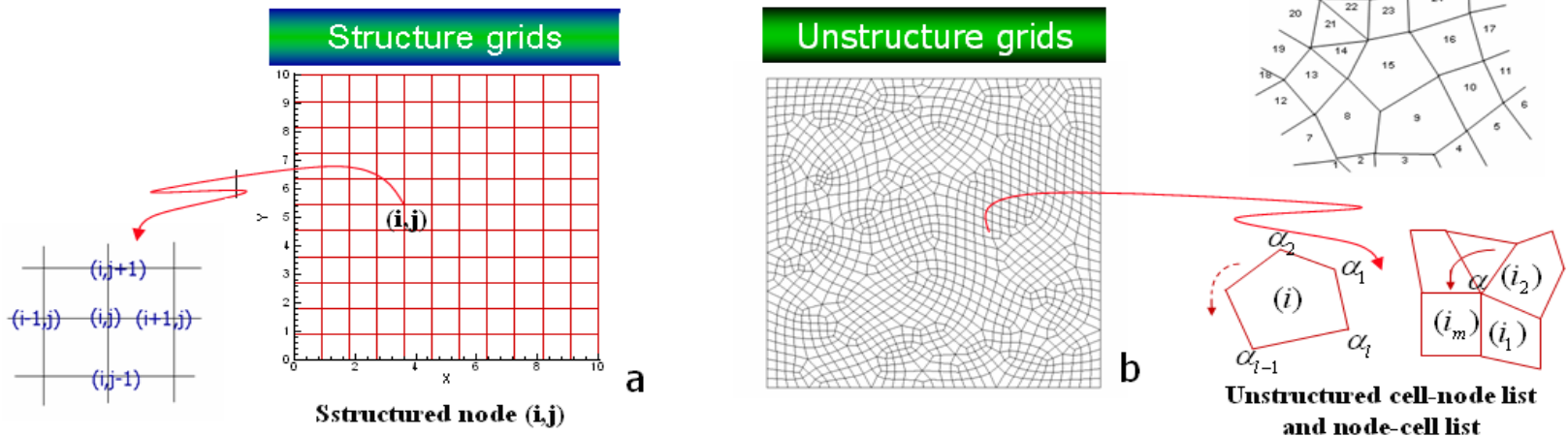


Fig.6 Management of the grids

# Polygonal meshes and motivation(3)

## ➤ Polygonal meshes

- The motivation of this work is the development methods for changing connectivity of mesh technology. A key component of the changing connectivity of mesh technology is polygonal meshes.

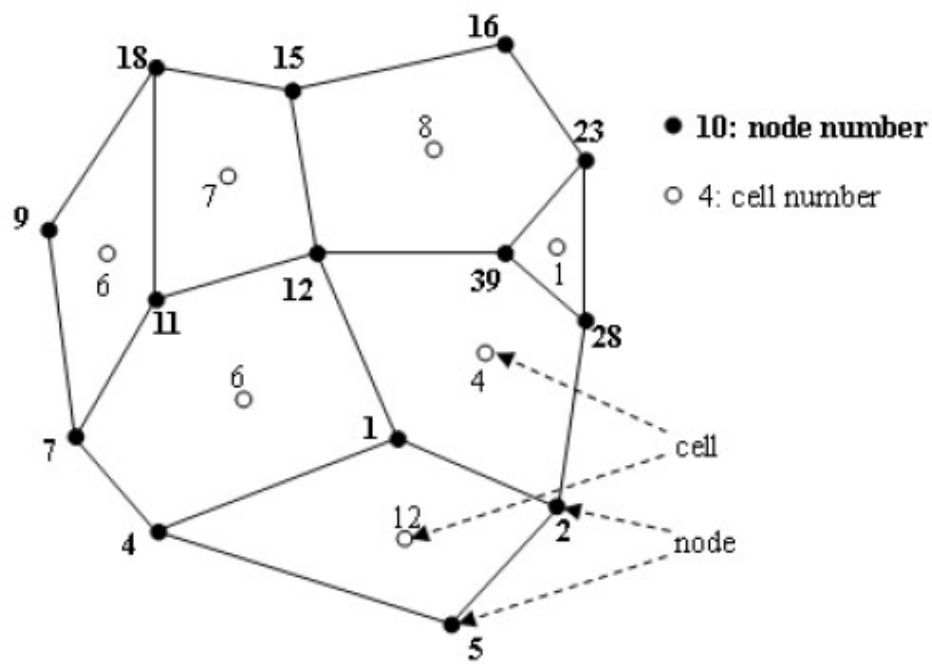


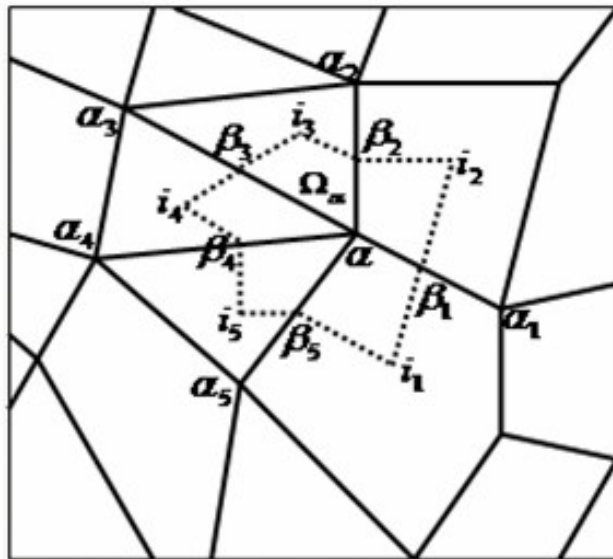
Fig.7 Polygonal mesh and notations. The set of nodes for cell  $c=12$  is  $CNL(C=12)=\{5,2,1,4\}$ , and the set of cells sharing node,  $n=39$  is  $NCL(n=39)=\{1,8,4\}$

# The changing connectivity of mesh (1)



## ➤ Computational scheme

The computational method is based on the arbitrary unstructured polygonal grid. The **Lagrangian finite volume method** and various viscosity such as classical Von Neumann-Richtmyer viscosity (the quadratic form viscosity), Landshoff viscosity (linear viscosity), shock wave viscosity, subzonal pressure method, artificial heat exchange in eliminating nonphysical deformation of Lagrangian mesh.



$$u_a^{n+1} = u_a^n + \frac{\Delta t^n}{B_a^n} \sum_{k=1}^{N_k} \left\{ -(p+q)_{\beta_{k-1}}^n (x_k^n - x_{\beta_{k-1}}^n) + (p+q)_{\beta_k}^n (x_{\beta_k}^n - x_k^n) \right\}$$

$$v_a^{n+1} = v_a^n + \frac{\Delta t^n}{B_a^n} \sum_{k=1}^{N_k} \left\{ +(p+q)_{\beta_{k-1}}^n (x_k^n - x_{\beta_{k-1}}^n) + (p+q)_{\beta_k}^n (x_{\beta_k}^n - x_k^n) \right\}$$

Where  $B_a^n = \mathbf{e} \frac{\rho_a^n A_a^n}{V_a^n}$ ,  $q$  is the artificial viscosity,

$\Delta t$  is the time step, the subscript denotes the Lagrangian cell or vortex, the superscript refers to the iteration number,  $A$  is the area of the mesh.

Fig.8 Control volume  $\Omega_a$  of momentum equation

# The changing connectivity of mesh(2)



- The changing connectivity of mesh (topology transformation) is allowed during numerical simulation.

For example, in Figure 2, during the calculation processes, when the node  $\alpha_k$  is equal to the node  $\alpha_{j+1}$  ( $\alpha_k = \alpha_{j+1}$ ) of the *mesh-i* at  $t^{n+1}$ , the concave-point  $\alpha_j$  cut across the edge  $\alpha_{j+1} \rightarrow \alpha_j$  in *mesh-i* (only neighbor edge  $\alpha_k \rightarrow \alpha_{k+1}$  with  $\alpha_k$ ), connectivity of the *mesh-i* to change, which to eliminate edge  $\alpha_k \rightarrow \alpha_{k+1}$  of the *mesh-i*, is defined as cut down edge to *mesh-i* on the left. From Figure 2, it is clear that topological operations with logically quadrilateral element are changed triangles element.

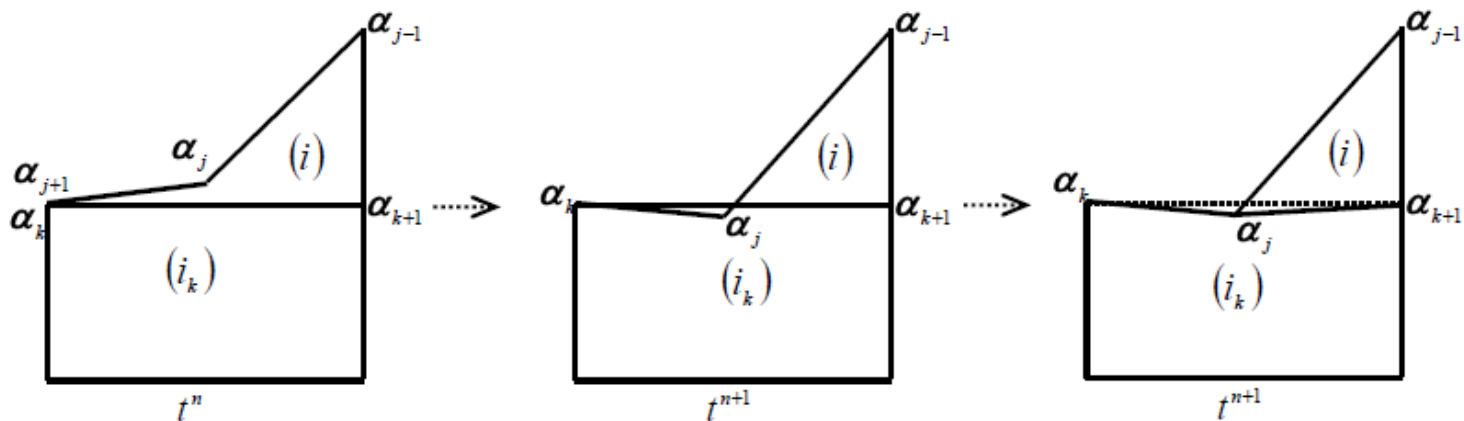


Figure 2 Cutting down edge to *mesh-i* on the left

# The changing connectivity of mesh(3)

For example, In the Figure 3, during the calculation processes, when the concave-point  $\alpha_j$  at  $t^{n+1}$  cut across the edge  $\alpha_k \rightarrow \alpha_{k+1}$  in  $mesh-i$ , connectivity of the  $mesh-i$  to change, which to eliminate edge  $\alpha_{k+1} \rightarrow \alpha_k$  of the  $mesh-i$ , is defined as merging to  $mesh-i$ , or which to refine edge  $\alpha_{k+1} \rightarrow \alpha_k$  of the  $mesh-i$ , is defined as refining to  $mesh-i$ .

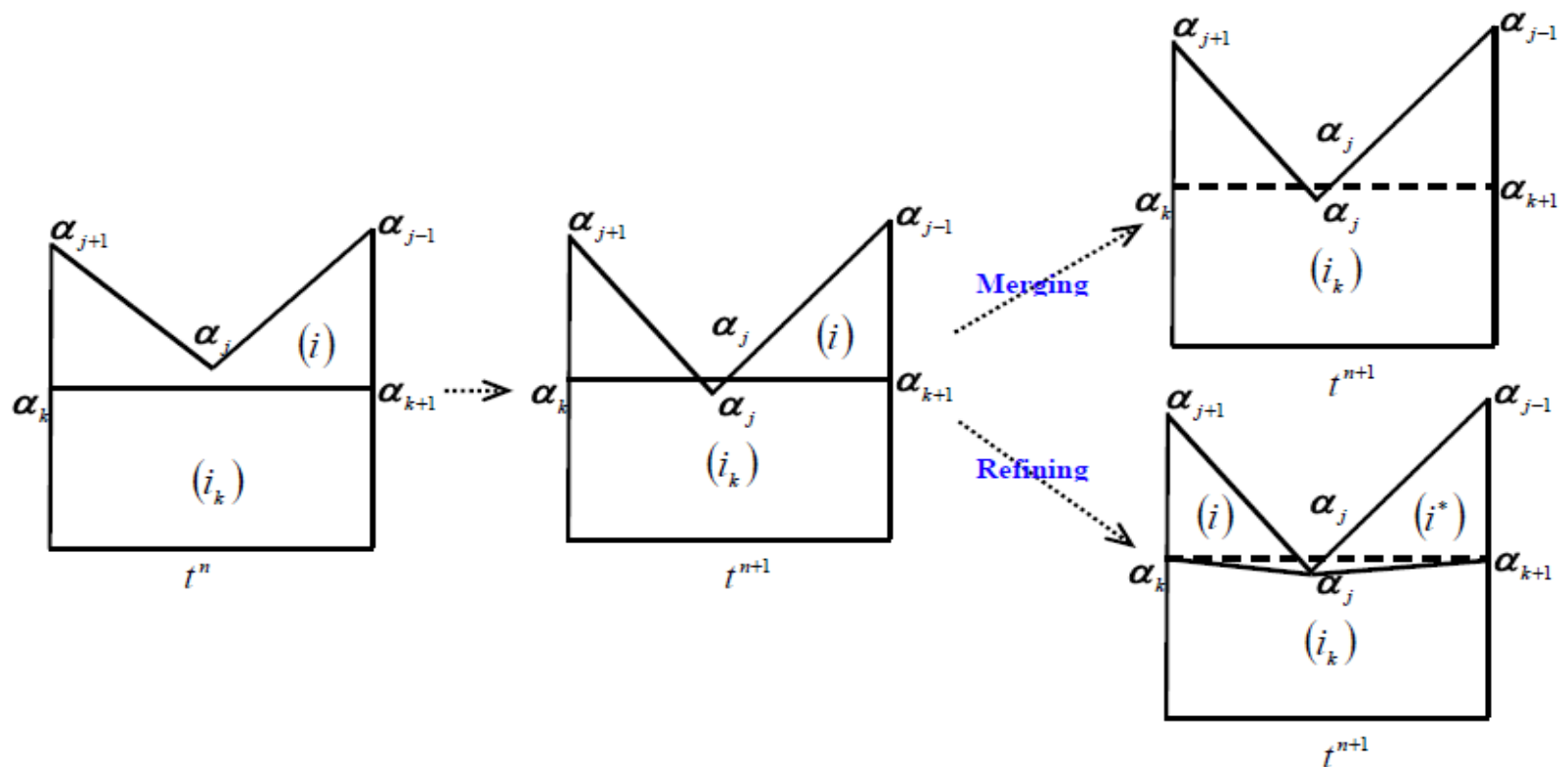


Figure 3 Merging or refining to  $mesh-i$

# The changing connectivity of mesh(4)

- This approach has successfully been implemented in LAD2D software, and applied to close gap (see Figure 4) and to handle the large deformation mesh(see Figure 5) during numerical simulation.

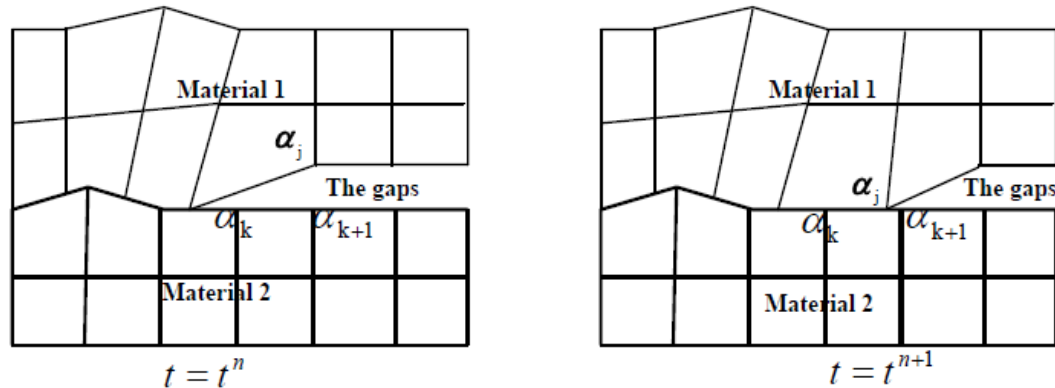


Figure 4 The changing connectivity of mesh applies to closing slide surface with void cavity

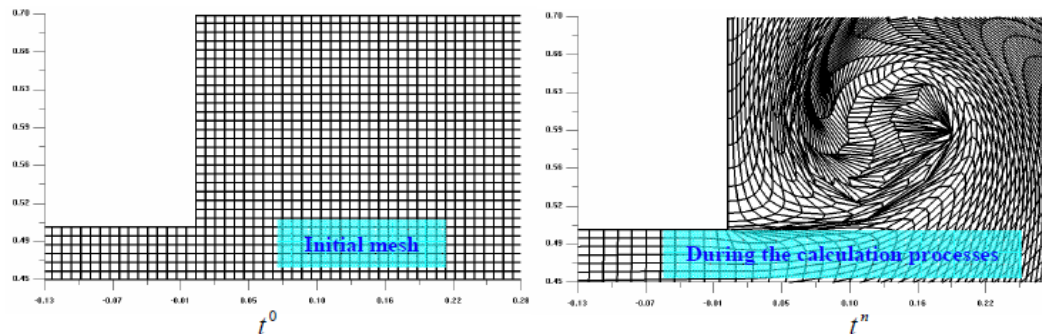


Figure 5 The changing connectivity of mesh applies to handle the large deformation mesh

# LAD2D Code (1)



IAPCM

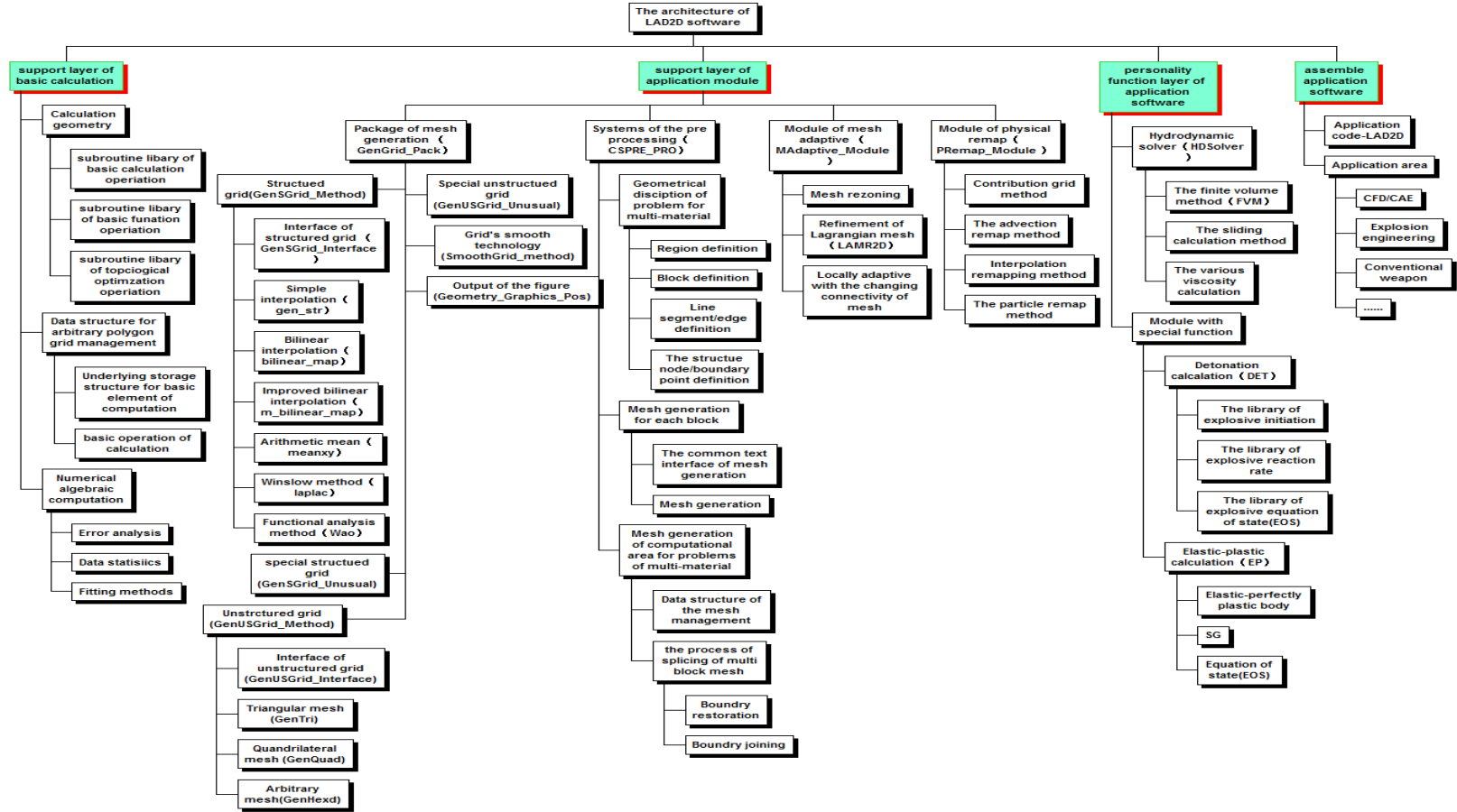
## ➤ The main features of LAD2D

- **LAD2D: Lagrange Adaptive hydroDynamics code in Two Dimensions**
- Solve multi-material, large deformation elastic-plastic flows;
- Object-oriented programming , generality, reliability and maintainability, good modification;
- Fortran 90 and C ++ programming language;
- LAD2D consists of the main body and several independent general modules。 The main body includes a control, a pre-process, a central operation, a grid, a post-process sub-systems, a common data module and a error process sub-system. The four independent general modules are grid generation(GRID2D), adaptive mesh refinement (AMR2D), remapping (REMAP2D) and grid adaption (ADAP2D) ;
- More than 200,000 line statements。

# LAD2D Code (2)



➤ The LAD2D code architecture (see Figure 1)



**Including:** 1 support layer of basic calculation;  
module;

2 support layer of application

3 personality function layer of application software; 4 assemble application software



# Numerical examples (1)

---

- To illustrate the effectiveness of our technique, three simulations are presented.
- The first comprises a detonation wave propagating through the channels with suddenly expending section.
- Next, the cavitations or void closure properties of the method are investigated by simulating sliding detonation model of one point initiation.
- Finally, the large deformation capabilities of the method are investigated with the simulation of a high velocity impact.

# Numerical examples (2)



## ➤ The diffraction problem of a detonation wave behind a backward-facing step

Diffraction of a detonation wave behind a backward-facing step is one of the fundamental topics in shock wave dynamics and is studied extensively by many researchers.

The computational domain  $\Omega$ , which is described in Figure 1.  $\Omega$  is split into two regions filled with the explosive PBX-9404 with parameters  $K=2.996$ ,  $D_J=8.88 \text{ km/s}$ ,  $\rho_0=1.84 \text{ g/cm}^3$ . The left region is  $\Omega_1 = [0, 3.0] \times [0, 0.5]$ , The right region is  $\Omega_2 = [3.0, 6.0] \times [0, 3.0]$ . The driver section is in the left part of the  $\Omega_1$ , the upper boundary is a solid-wall condition; the lower is an ax symmetric condition. The parameters  $A, B, R_1, R_2$  and  $\omega$  used for JWL are  $A=8.524$ ,  $B=0.1802$ ,  $R_1=4.6$ ,  $R_2=1.3$ ,  $\omega=0.38$ . The parameters  $n_b$  and  $\gamma_b$  are chosen as  $n_b=1.1$ ,  $\gamma_b=2.1$ . The structured mesh of  $180 \times 30$  elements is used to discretise the left region, and The structured mesh of  $180 \times 120$  elements is used to discretise the right region.

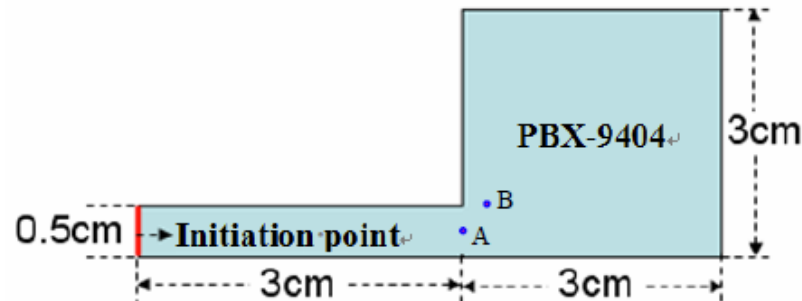


Fig.1 Computational domain for detonation wave behind a backward-facing steps, and in near corner containing Lagrangian reference point A and point B.

# Numerical examples (3)



## ➤ diffraction of a detonation wave behind a backward-facing step

The changing connectivity of mesh technology was used during the computational process.

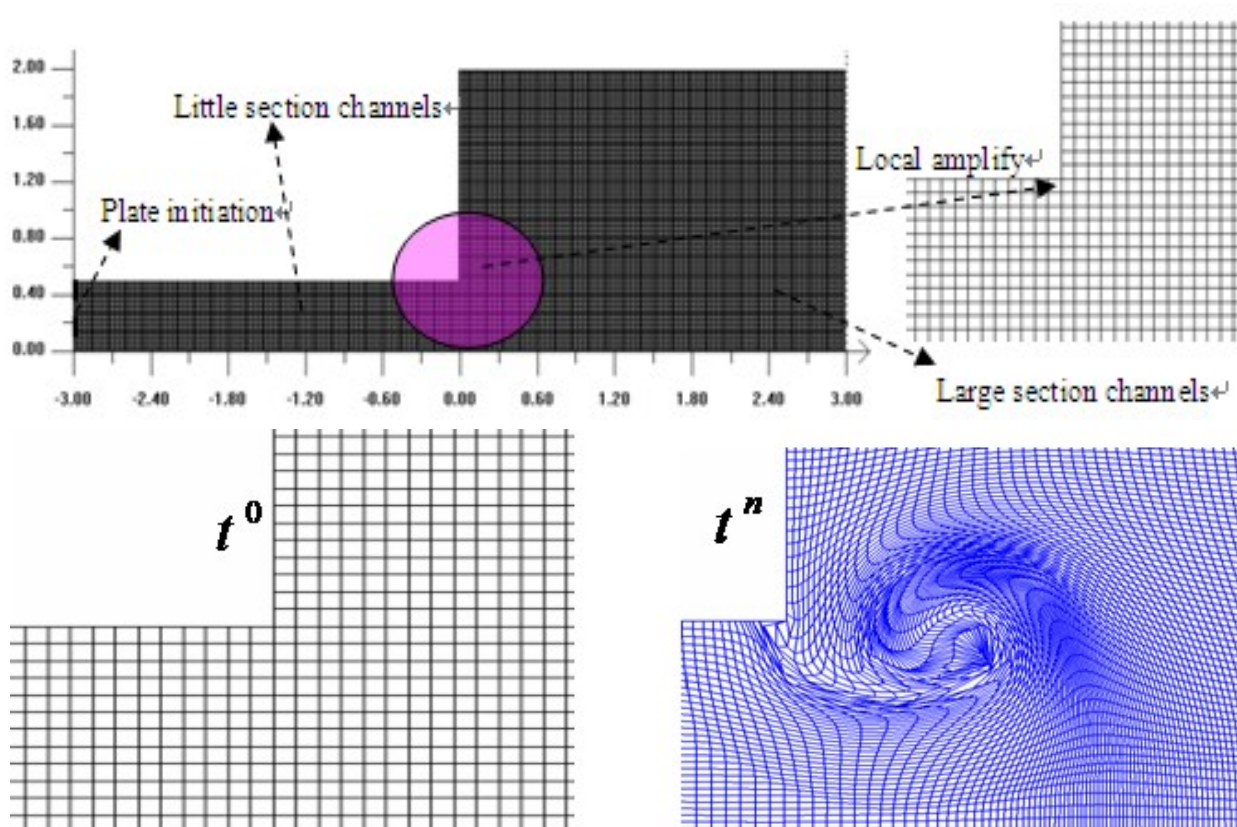


Figure 2 The computational grids changed from  $t^0$  to  $t^n$

# Numerical examples (4)



IAPCM

## ➤ diffraction of a detonation wave behind a backward-facing step

Figure 3 shows the computing mesh (upper) and density contours (lower) at three times. Diffraction through the  $90^\circ$  corner also generates a stronger corner vortex. We compare numerical results with experimental data by using high-speed schlieren photography, which coincide qualitatively.

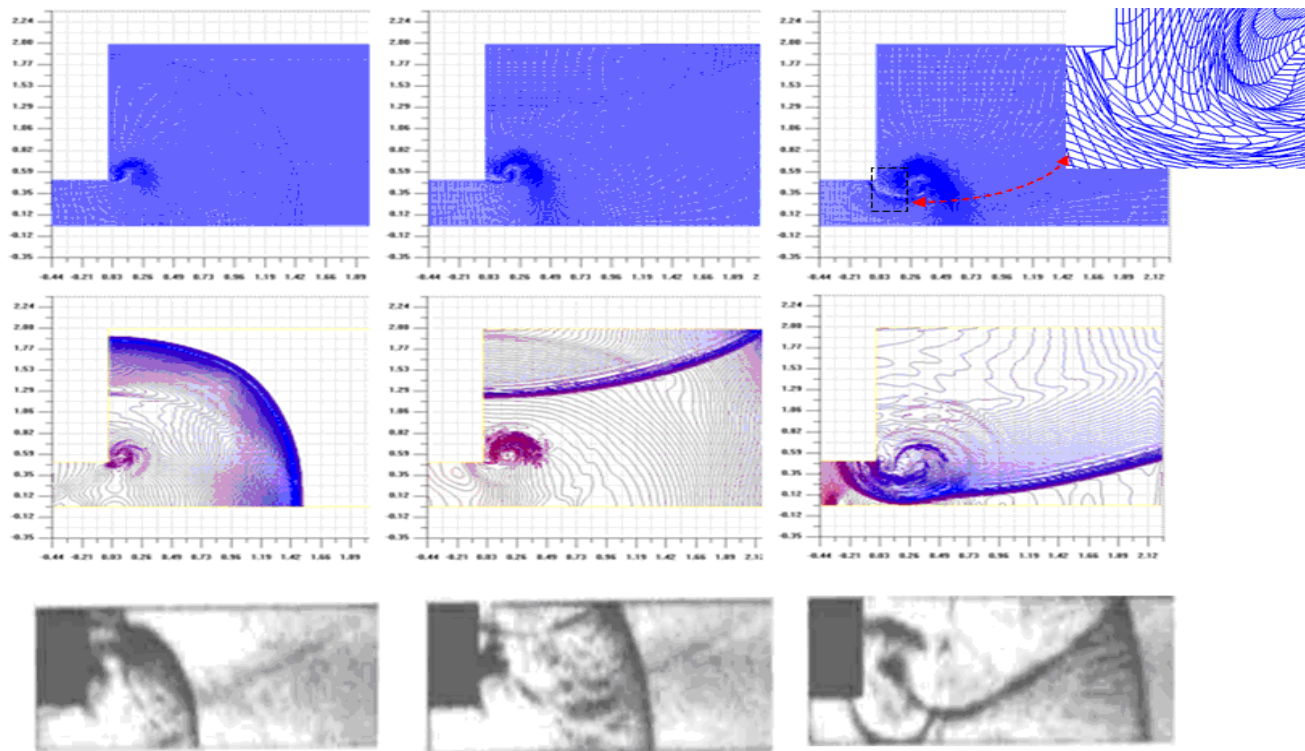


Fig.3 The comparison between the numerical results and the experimental data (upper: mesh; center: contours of density; under: experimental results)

# Numerical examples (5)



## ➤ The sliding detonation model of one point initiation

The detailed structure of this model can be seen in the Figure 1. Five regions exist in this model, from the inner to the outer, it is filled with gas (vacuum zone), tungsten(W), aluminum(Al), explosive(PBX9404), and tungsten(W). The radius of these regions are  $R_0 = 10.0\text{cm}$ ,  $R_1 = 10.2\text{cm}$ ,  $R_2 = 10.5\text{cm}$ ,  $R_3 = 13.2\text{cm}$ ,  $R_4 = 13.5\text{cm}$  respectively.

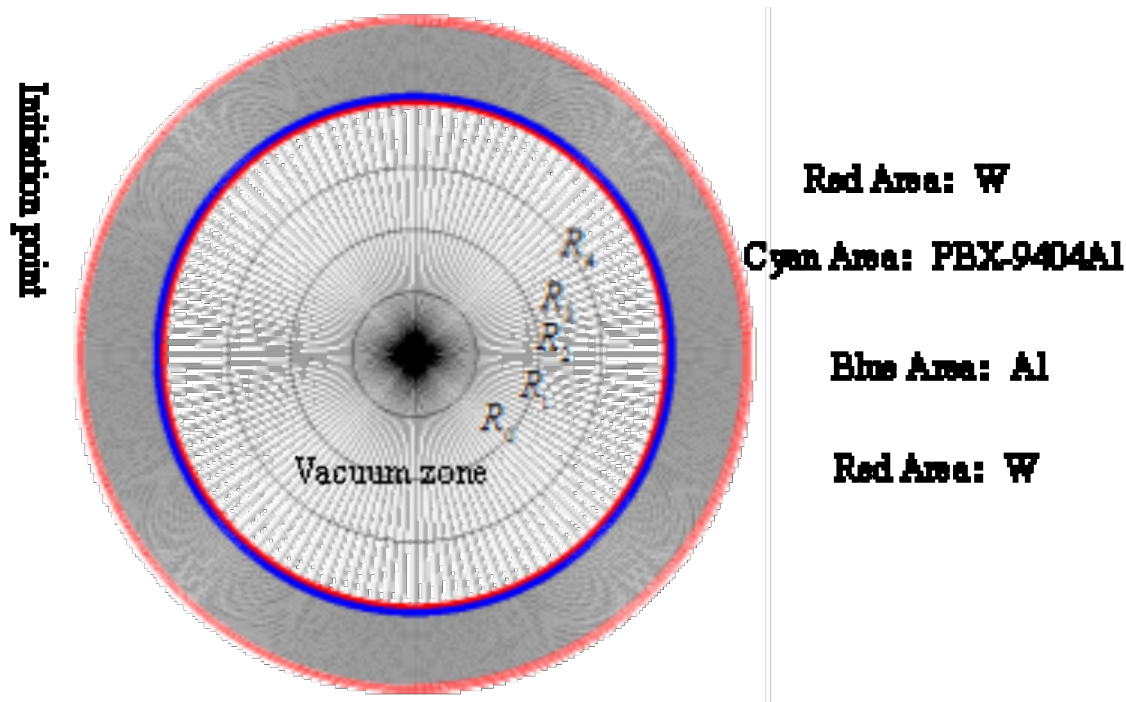


Fig.1 The computational domain of one point initiation

# Numerical examples (6)



## ➤ The sliding detonation model of one point initiation

In the simulation process, the central vacuum zone used the changing connectivity of mesh technology. Figure 2 shows process of the central cavity closing. The point-a and point-b on the Figure 2 gradually closed cavity by using the changing connectivity of mesh technology.

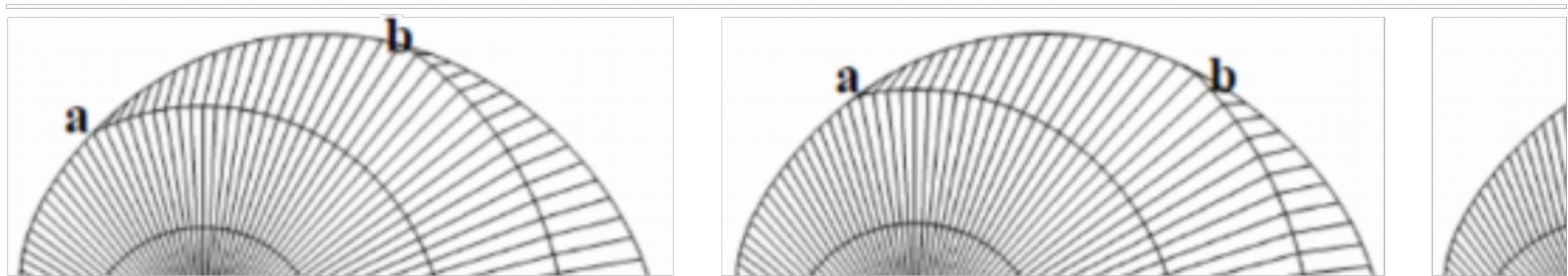


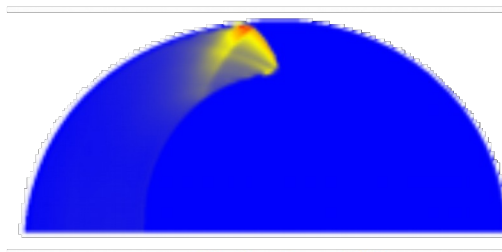
Fig.2 The computational grids changed at central vacuum zone

# Numerical examples (7)



## ➤ The sliding detonation model of one point initiation

Figure 3 display the distributions of pressure at increasing times, which also shows procedure of detonation wave propagation. In the simulation process, the central vacuum zone used the changing connectivity technology of mesh. We can see from Figure 3 that the detonation wave propagation is reasonable by the changing connectivity technology of mesh, it is can be used to verify the LAD2D software.



(a)  $t = 20 \mu s$

(b)  $t = 25 \mu s$

(c)  $t = 30 \mu s$

(d)  $t = 35 \mu s$

(e)  $t = 40 \mu s$

(f)  $t = 45 \mu s$

Fig.3 Panels (a)-(f) display the distributions of pressure  $P$  at increasing times

# Numerical examples (8)



## ➤ The high-velocity impact simulations

The computational domain employed in this simulation is shown in Figure 1. The initial meshes, which completely fills the domain, is constructed from a number of elements. The unstructured mesh of 3244 elements is used to discretise the circular projectile, which is 10mm in diameter. The structured mesh of  $15 \times 100$  elements is used elsewhere to discretise the rectangular target ( $2 \times 50 \text{ mm}$ ) (see Figure 2). Again the stiffened gas EOS is used for both steel and aluminum (see Table 1 for material properties). A CFL number of 0.3 is used in timestep control, and the changing connectivity of mesh technology is used during numerical simulation.

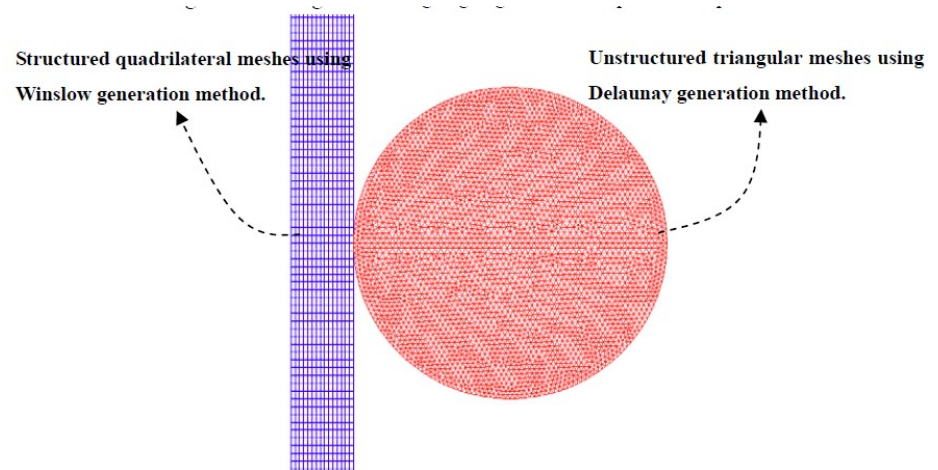
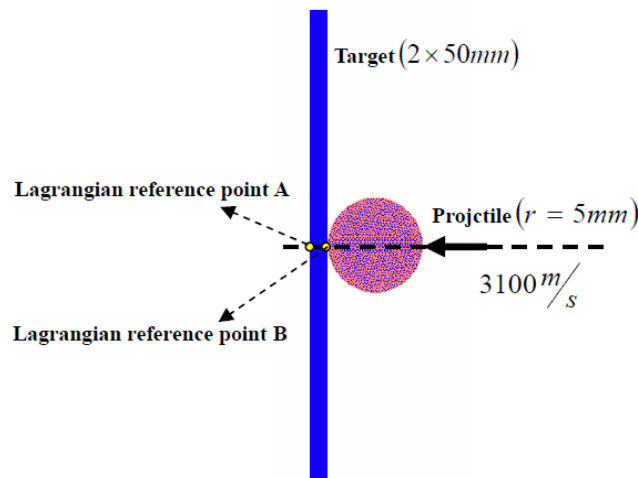


Fig.1 Domain configuration for the high-velocity impact of steel projectiles on a thin aluminum target. and in target containing Lagrangian reference point A and point B.

Fig.2 The initial mesh distribution is unstructured mesh of 3244 elements for steel projectile and structured mesh of  $15 \times 200$  elements for aluminum

# Numerical examples (9)



## ➤ The high-velocity impact simulations

The stiffened gas equation of state where the pressure  $P$  and sound speed  $c_s$  are given in terms of the density  $\rho$  and the specific internal energy  $e$  by

$$P = c_0^2(\rho - \rho_0) + (\gamma - 1)\rho e, \quad (1)$$

$$c_s = c_0 \left[ \gamma - (\gamma - 1) \frac{\rho_0}{\rho} \right] + \gamma(\gamma - 1)e. \quad (2)$$

Material properties utilized in the three simulations are listed in Table 1.

Table 1 Material property for aluminum and steel

property	Aluminum	Steel
Density, $\rho \left( \frac{\text{g}}{\text{cm}^3} \right)$	2.785	7.900
Bulk sound speed, $c_0 \left( \frac{\text{cm}}{10 \mu\text{s}} \right)$	5.328	4.600
Gruneisen parameter, $\gamma$	2.000	2.170
Shear modulus, $G(\text{kPa})$	$2.760 \times 10^7$	$8.530 \times 10^7$
Yield stress, $Y_0(\text{kPa})$	$0.300 \times 10^6$	$0.979 \times 10^6$

# Numerical examples (10)



## ➤ The high-velocity impact simulations

Figure 3 shows part of the Lagrange computational mesh with the changing connectivity of mesh technology in the vicinity of the projectile at  $1.0\mu s$  and  $2.0\mu s$ . Even at this early time, Lagrangian motion of the mesh with the changing connectivity of mesh technology, and the formation of ejecta from both the projectile and target, is evident.

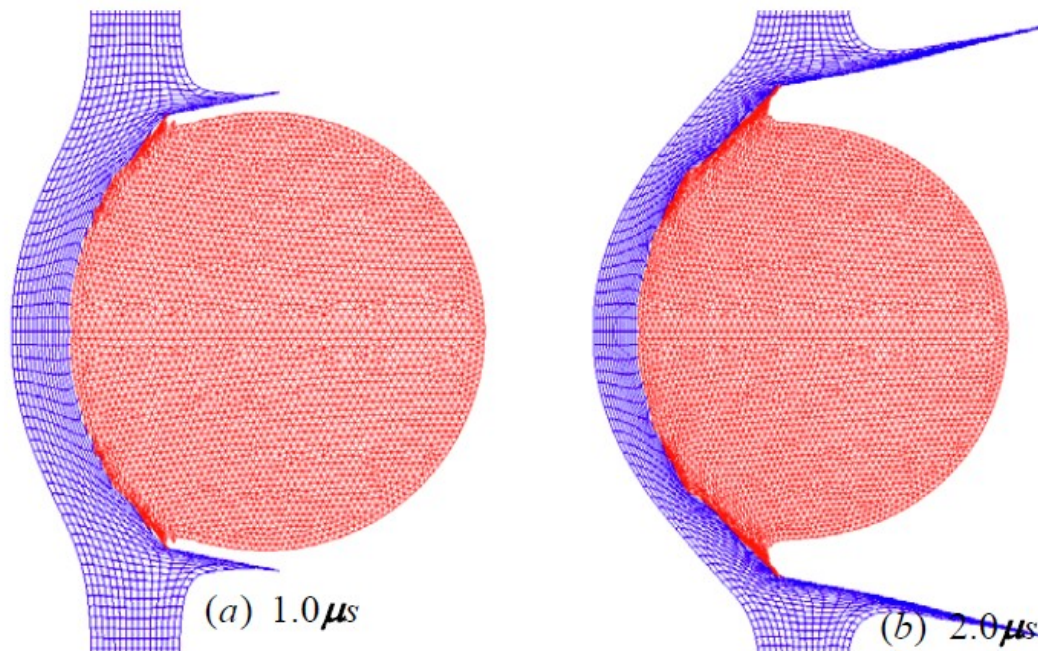


Fig.3 Detail of Lagrange computational mesh with the changing connectivity of mesh technology for the high-velocity impact simulation of steel projectile on the aluminum target

# Numerical examples (11)



## ➤ The high-velocity impact simulations

Transient results to an elapsed time of  $8.0\mu s$  from initial impact are shown in Figure 4 for a steel projectile striking an aluminum target. Figure 4a-4h shown the material geometry and mesh distributions by LAD2D software.

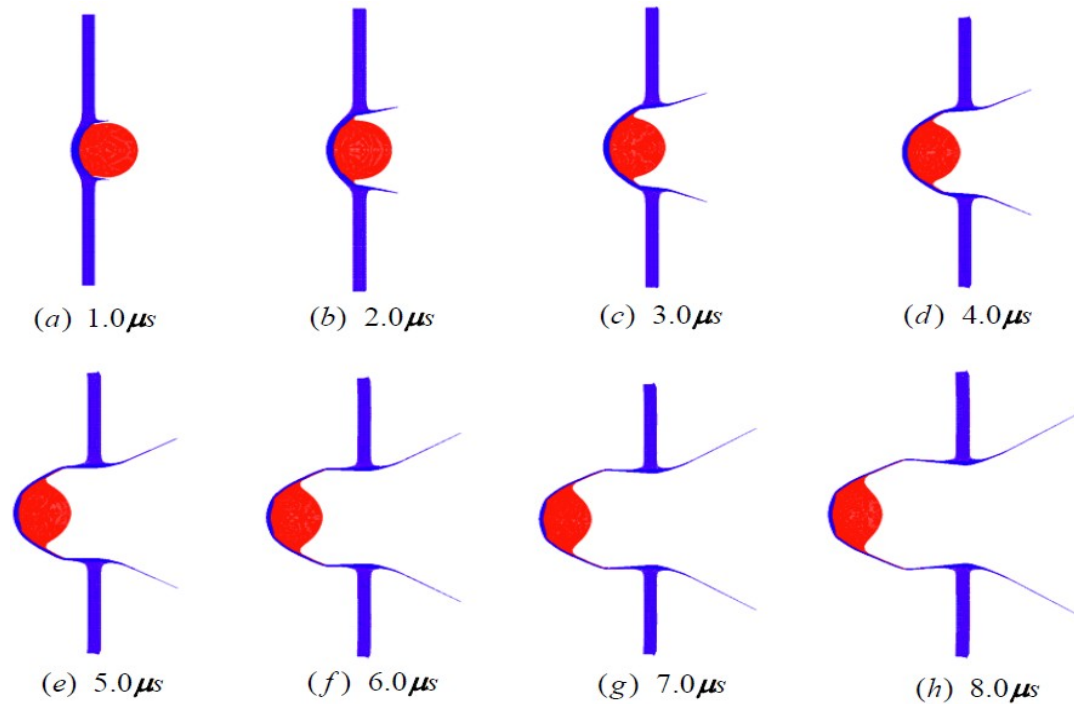


Fig.4 Transient results illustrating material deformation and geometry structures for the high-velocity impact of a circular steel projectile on an aluminum target

# Numerical examples (12)



## ➤ The high-velocity impact simulations

Figure 5 shown time histories for high-velocity impact simulation, recorded at Lagrangian reference point A and B within the target (see Fig.1).

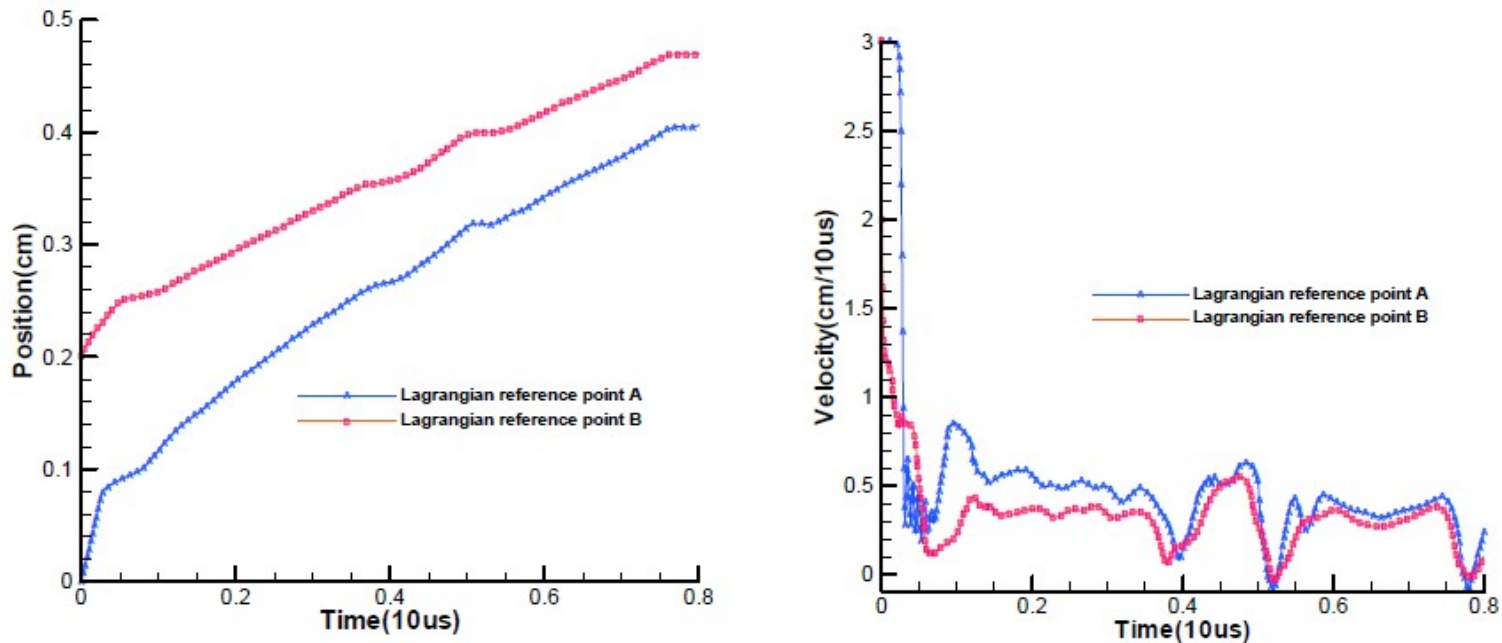


Fig.5 Time histories for high-velocity impact simulation, recorded at Lagrangian reference point A and B within the target (see Fig.1)

The three simulations shown the large deformation capabilities of the Lagrange method with the changing connectivity of mesh technology.

# Conclusions

---



IAPCM

- Lagrangian method is a main simulation tool in multifluids under high temperature and high pressure.
- Based on the unstructured arbitrary polygonal mesh, **the new methods with the changing connectivity of mesh technology to to handle the large deformation mesh and to close gap was presented during numerical simulation processes.**
- The three numerical examples have demonstrated that our new method has strong simulation the large deformation capabilities.

# References



IAPCM

1. Wang R L, Jiang S, Mathematical methods for uncertainty quantification in nonlinear multi-physics systems and their numerical simulations, *Sci Sin Math*, 2015, 45: 723–738, doi: 10.1360/N012014-00115. (in Chinese)
2. D.J. Benson, Computational methods in Lagrangian and Eulerian hydrocodes, *Comp. Meth. Appl. Mech. Engrg.*, 99, 235-394, 1992.
3. J.C. Campbell, M.J. Shashkov, A Compatible Lagrangian Hydrodynamics Algorithm for Unstructured Grids. *Selcuk J. Appl. Math.*, 4(2): 53-70, 2003.
4. WANG Ruili, LIN Zhong, WEN Wanzhi and so on, Development and application of adaptive multi-media Lagrangian fluid dynamics software LAD2D, *Computer Aided Engineering*, 2014, 23 (2): 1-7. (in Chinese)
5. W. Ruili, Z. Shudao and L. Quan, One Method of Constructing Manufactured Solutions to 2D Hydrodynamics Euler Equations, *Proceedings of the International Conference on Numerical Analysis and Applied Mathematics 2014 (ICNAAM-2014)*, AIP Conf. Proc. 1648, 030028-1–030028-4; doi: 10.1063/1.4912345.6.
6. Ruili Wang, Xiao Liang, Wenzhou Lin, Xuezhe Liu, Yunlong Yu, Verification and validation of the detonation computational fluid dynamics model, *Defect and Diffusion Forum*, 2016, ISSN: 1662-9507, Vol. 366, pp 40-46, doi:10.4028/www.scientific.net/DDF.366.40.
7. C.J. Roy, C.C. Nelson, T.M. Smith, C.C. Ober, Verification of Euler/Navier–Stokes codes using the method of manufactured solutions, *Int. J. Numer. Meth. Fluids*, 2004, 44 (6) : 599–620.
8. J.C. Helton, Conceptual and Computational Basis for the Quantification of Margins and Uncertainty, SAND2009-3055, 2009.
9. E.L. Lee, H.C. Hornig, Equation of state of detonation product gases, In: *Combustion Inst, 12th Symposium (International) on Combustion*, 1969, 12: 493-499.
10. S. Ohyagi, T. Obara, S. Hoshi, P. Cai, T. Yoshihashi, Diffraction and re-initiation of detonations behind a backward-facing step, *Shock Waves*, 2002, 12: 221-226.
11. B.P.Howell, G.J.Ball, A free-Lagrange augmented Godunov method for the simulation of Elastic-Plastic solids, *Journal of computational physics*, 2002, 175:128-167.

Thank you !

